

Insulin Causes Hyperthermia by Direct Inhibition of Warm-Sensitive Neurons

Manuel Sanchez-Alavez,¹ Justin V. Tabarean,¹ Olivia Osborn,¹ Kayo Mitsukawa,¹ Jean Schaefer,² Jeffrey Dubins,² Kristina H. Holmberg,³ Izabella Klein,¹ Joe Klaus,¹ Luis F. Gomez,⁴ Hartmuth Kolb,⁴ James Secrest,⁴ Jeanine Jochems,⁵ Kevin Myashiro,⁵ Peter Buckley,⁵ John R. Hadcock,² James Eberwine,⁵ Bruno Conti,¹ and Tamas Bartfai¹

OBJECTIVE—Temperature and nutrient homeostasis are two interdependent components of energy balance regulated by distinct sets of hypothalamic neurons. The objective is to examine the role of the metabolic signal insulin in the control of core body temperature (CBT).

RESEARCH DESIGN AND METHODS—The effect of preoptic area administration of insulin on CBT in mice was measured by radiotelemetry and respiratory exchange ratio. In vivo 2-[¹⁸F]fluoro-2-deoxyglucose uptake into brown adipose tissue (BAT) was measured in rats after insulin treatment by positron emission tomography combined with X-ray computed tomography imaging. Insulin receptor-positive neurons were identified by retrograde tracing from the raphe pallidus. Insulin was locally applied on hypothalamic slices to determine the direct effects of insulin on intrinsically warm-sensitive neurons by inducing hyperpolarization and reducing firing rates.

RESULTS—Injection of insulin into the preoptic area of the hypothalamus induced a specific and dose-dependent elevation of CBT mediated by stimulation of BAT thermogenesis as shown by imaging and respiratory ratio measurements. Retrograde tracing indicates that insulin receptor-expressing warm-sensitive neurons activate BAT through projection via the raphe pallidus. Insulin applied on hypothalamic slices acted directly on intrinsically warm-sensitive neurons by inducing hyperpolarization and reducing firing rates. The hyperthermic effects of insulin were blocked by pretreatment with antibodies to insulin or with a phosphatidylinositol 3-kinase inhibitor.

CONCLUSIONS—Our findings demonstrate that insulin can directly modulate hypothalamic neurons that regulate thermogenesis and CBT and indicate that insulin plays an important role in coupling metabolism and thermoregulation at the level of anterior hypothalamus. *Diabetes* 59:43–50, 2010

From ¹The Harold L. Dorris Neurological Research Institute, Department of Molecular and Integrative Neurosciences, The Scripps Research Institute, La Jolla, California; ²Pfizer Global Research, Groton, Connecticut; ³Pfizer, Experimental Biological Sciences, Kent, U.K.; ⁴Siemens Medical Solutions, Healthcare Imaging and Information Technology, Molecular Imaging Biomarker Research, Culver City, California; and the ⁵Department of Pharmacology, School of Medicine, University of Pennsylvania, Philadelphia, Pennsylvania.

Corresponding author: Olivia Osborn, olivial@scripps.edu.

Received 30 July 2009 and accepted 11 October 2009. Published ahead of print at <http://diabetes.diabetesjournals.org> on 21 October 2009. DOI: 10.2337/db09-1128.

M.S.-A., I.V.T., and O.O. contributed equally to this work.

© 2010 by the American Diabetes Association. Readers may use this article as long as the work is properly cited, the use is educational and not for profit, and the work is not altered. See <http://creativecommons.org/licenses/by-nc-nd/3.0/> for details.

The costs of publication of this article were defrayed in part by the payment of page charges. This article must therefore be hereby marked "advertisement" in accordance with 18 U.S.C. Section 1734 solely to indicate this fact.

Core body temperature (CBT) and nutrient homeostasis are important components of energy balance that can affect each other by mechanisms that are not clearly understood. In homeotherms, both are regulated centrally by distinct hypothalamic nuclei and neurons. The preoptic area (POA) is essential for the regulation of CBT (1). This region contains temperature- (warm and cold) sensitive neurons that are considered pivotal in sensing and responding to local- and skin-temperature changes (2,3). Nutrient homeostasis is regulated by different hypothalamic regions, the paraventricular and the arcuate nucleus, that contain neurons responding to changes in the level of glucose, lipids, ghrelin, leptin, and insulin, respectively (4,5). Intracerebroventricular injection of insulin reduced the unit activity of POA neurons sensitive to peripheral changes in scrotum temperature, indicating that this hormone may modulate thermoregulatory responses (6). Because the insulin receptor was detected in the POA (5,7–9), we hypothesized that insulin could elevate CBT by directly acting on temperature-sensitive neurons in the POA. Furthermore, our data (unpublished results) on single-neuron chipping of temperature-/warm-sensitive neurons in the POA showed the presence of insulin receptor mRNA in these neurons whose firing activity is inversely correlated with the activation of thermogenesis in brown adipose tissue (BAT) (10).

RESEARCH DESIGN AND METHODS

All procedures were approved by the Institutional Animal Care and Use Committee of the Scripps Research Institute and were carried out on 3- to 4-month-old male C57BL/6J mice. Animals were maintained on regular chow (Harlan Teklad LM-485 Diet 7012; carbohydrate 65% kcal, fat 13%, metabolizable energy 3.41 kcal/g). Access to food and water was ad libitum, and the light:dark cycle was 12:12 h with lights on at 7:00 A.M.

For telemetry studies, male mice were anesthetized with isoflurane (induction 3–5%, maintenance 1–1.5%) and surgically implanted with radio telemetry devices (TA-F20; Data Sciences) into the peritoneal cavity for CBT and locomotor activity measurement. Mice were allowed to recover for 2 weeks and then were submitted for freely moving telemetry recording (each group $n = 4–6$) for 7 days. Mice were individually housed in a Plexiglas cage in a room maintained at $25 \pm 0.5^\circ\text{C}$ on a 12:12 h light:dark cycle (lights on at 6:00 A.M.) with ad libitum access to food and water. The cages were positioned onto the receiver plates (RPC-1; Data Sciences), and radio signals from the implanted transmitter were continuously monitored and recorded. CBT and locomotor activity (number of horizontal movements) were continuously monitored with a fully automated data acquisition system (Dataquest ART; Data Sciences). Recordings were made for ≥ 72 h before treatment to ascertain that baseline levels of temperature were stable and that no ongoing febrile response confounds the results.

Insulin (I1507; Sigma, St. Louis, MO) was predissolved in saline and subsequently diluted in artificial cerebrospinal fluid (aCSF). Phosphatidylinositol 3-kinase inhibitor (PI3K-I), LY294002 (70920; Cayman Chemical, Ann

Arbor, MI), was predissolved in DMSO and subsequently diluted in aCSF (final concentration 5% DMSO). Injections of insulin (or vehicle aCSF), PI3K-I (or vehicle aCSF with 5% DMSO), or insulin antibodies (I8510; Sigma, St. Louis, MO) (or vehicle aCSF) were administered directly to the POA through the POA-implanted cannula (anterior-posterior [AP] from bregma = 0.38 mm, lateral [Lat] = midline, ventral [V] = 3.8 mm, cannula 26 GA, 10 mm length) using an injector (33 GA, protruding 0.4 mm beyond the tip of the cannula, total length 10.4 mm) connected to plastic tubing and a microsyringe (10 μ l) in a volume of 0.5 μ l over a period of 5 min to allow diffusion ($n = 5$ mice per group).

Indirect calorimetry was performed simultaneously in acclimated, singly housed, standard diet-fed mice using a computer-controlled open-circuit system (Oxymax System) that is part of an integrated Comprehensive Lab Animal Monitoring System (CLAMS; Columbus Instruments, Columbus, OH). Animals are tested in clear respiratory chambers (20 \times 10 \times 12.5 cm) with a stainless steel elevated wire floor. Each of these chambers is equipped with a food tray connected to a balance. Room air is passed through chambers at a flow rate of \sim 0.5 l/min. Exhaust air from each chamber is sampled at 30-min intervals for 1 min. Sample air is sequentially passed through O₂ and CO₂ sensors (Columbus Instruments) for determination of O₂ and CO₂ content, from which measures of oxygen consumption (VO₂) and carbon dioxide production (VCO₂) are estimated. Outdoor air reference values are sampled after every four measurements. Gas sensors are calibrated prior to the onset of experiments with primary gas standards containing known concentrations of O₂, CO₂, and N₂ (Airgas Puritan Medical, Ontario, Canada). Respiratory exchange ratio (RER) is calculated as the ratio of VCO₂ to VO₂. Energy expenditure measures (VO₂, VCO₂, and heat formation [(3.815 + 1.232 \times RER) \times VO₂ (in liters)]) are corrected for estimated effective metabolic mass per Kleiber power function. Mice undergoing indirect calorimetry are acclimated to the respiratory chambers for 3–4 days before the onset of study. Data are recorded under ambient room temperature clamped at 25°C, beginning from the onset of the light cycle, 24 h/day for 3 days.

Positron emission tomography and computed tomography imaging. Positron emission tomography (PET)/computed tomography (CT) imaging in this study was carried out with 2-[¹⁸F]fluoro-2-deoxyglucose (¹⁸F-FDG) on 12-week-old male Sprague Dawley rats (mean body wt 250 g). Rats are known to have a relatively large amount of BAT in the interscapular region and thus are often used in research for BAT activation (11). Each rat received 18.5 MBq of ¹⁸F-FDG via intraperitoneal injection, and 30 min later they were anesthetized with isoflurane (5% induction, 1–2% maintenance) and imaged with a combined PET/CT scanner (Siemens Medical Solutions) designed for small rodents at baseline and after microinjection of insulin into the preoptic area (AP = -0.9, lat = midline, V = 8.0 mm from dura) at 15, 30, 60, and 180 min. In brief, CT for attenuation correction and 5-min emission PET were performed, followed by thin-slice (1.5 mm thick) CT. PET and thin-slice CT images were reconstructed as 35-cm field-of-view images, and the PET and CT image sections at the same location were manually fused using image analysis software (Photoshop 6.0; Adobe Systems). The mild ¹⁸F-FDG uptake in skin and the contours of normal organs were used as landmarks. The PET and CT images were also intrinsically registered because of their acquisition on the dedicated PET/CT scanner. ¹⁸F-FDG uptake in interscapular BAT was evaluated using the PET, CT, and fused PET/CT images. Animal's body temperature was maintained at 37°C by a heat lamp (Temperature Controller RET-3 Temperature probe and HL-1 Heat Lamp; Physitemp Instruments, Clifton, NJ) in between periods of recording to avoid hypothermia during isoflurane anesthesia.

PET data were analyzed by visual interpretation of coronal, sagittal, and transverse slices alone and in cross-referenced situations. When ¹⁸F-FDG PET uptake increase was observed, two levels were identified in comparison with normal activity: moderate (more or less twice the activity in a reference region) or intense (markedly higher than the reference activity). PET and conventional imaging were interpreted separately, and the results were then compared with each other and, in certain cases, with the physiological information on hyperthermia. Bone scans and CT images were read independently by two nuclear medicine physicians and by two radiologists, respectively.

Slice preparation. The brain was quickly removed from C57BL/6 mice at 22–35 days old and submerged in ice-cold oxygenated (95% O₂/5% CO₂) normal aCSF; composition was (in mmol/l) NaCl 126, KCl 3.5, CaCl₂ 2, MgSO₄ 1, NaH₂PO₄ 1.25, NaHCO₃ 26, and glucose 10 (pH 7.4). Coronal slices (350 μ m thick) containing the POA were cut by a microslicer (Vibratome).

Patch clamp recording. Standard tight-seal recordings were performed in current clamp mode (I-fast) with an Axopatch 200B amplifier to record spontaneous action potentials. The external recording solution was aCSF. In some recordings 9 mmol/l glucose was replaced by 9 mmol/l mannitol. The pipette solution used was (in mmol/l) 130 K-gluconate, 10 KCl, 10 HEPES, 2 MgCl₂, 0.5 EGTA, 2 ATP, and 1 GTP (pH 7.4). Glass micropipettes were pulled

with a horizontal puller (P-87; Sutter Instruments, Novato, CA) using borosilicate glass. The electrode resistance after backfilling was 2–4 M Ω . All voltage measurements were corrected for the liquid junction potential (\sim -9 mV).

Temperature control. The temperature of the external solution was controlled with an HCC-100A heating/cooling bath temperature controller (Dagan Corporation), a fast temperature controller equipped with a Peltier element. To prevent changes induced in the electrode reference potential, the ground electrode was thermally isolated in a separate bath connected to the recording bath by a filter paper bridge.

Data acquisition and analysis. Recordings were digitized using a Digidata 1320A interface and analyzed using Pclamp9 (Axon Instruments, Union City, CA) software package and stored on the disk of a computer. After establishing whole-cell configuration (or perforated whole cell), the spontaneous activity of the neuron was recorded for 2–4 min to determine its control behavior (at 36–37°C), after which it was tested for temperature sensitivity with a temperature cycle of at least 33–39°C. The firing rate was determined for each 10-s interval and plotted against the temperature using Sigmaplot software. The criteria for classifying a neuron as being warm sensitive were the same as those used by previous investigations of temperature-sensitive neurons (1). Briefly, the thermal coefficient is defined as the slope of the linear regression of the firing rate plotted as a function of temperature. This plot was determined over a temperature range of \geq 3°C in which a neuron was most sensitive. A warm-sensitive neuron is defined as having a thermal coefficient \geq 0.8 impulses \cdot s⁻¹ \cdot C⁻¹. Neurons displaying nonreversible firing rate changes during changes in temperature were excluded.

Immunoblotting. Mice were anesthetized and POA tissues were obtained and homogenized in freshly prepared ice-cold radioimmunoprecipitation assay buffer (Thermo Scientific, IL) including 1 mmol/l Na₃VO₄, 1 mmol/l NaF, EDTA-free protease inhibitor, and PhosSTOP (Roche, Indianapolis, IN) 90 min after the injection of vehicle (aCSF) or insulin (0.03 IU) (Sigma) into the POA. Insoluble material was removed by centrifugation (15,000 *g*, 2 min) at 4°C. Sample buffer (0.125 mol/l Tris pH 6.8, 0.04% glycerol, 0.4% SDS, 0.01% β -mercaptoethanol, 0.02% Bromophenol Blue) was added and boiled for 5 min before separation in SDS-PAGE using 7.5% Ready Gel Tris-HCl gels (BioRad, Hercules, CA). Electrotransfer of proteins from the gel to nitrocellulose membrane was performed for 60 min at 100 V. The nitrocellulose transfers were probed with anti-insulin receptor- β subunit, anti-IGF-I receptor, and anti-phospho AKT (Ser473) antibodies from Cell Signaling Technology as well as β -actin (Millipore) for the normalization. Subsequently, the blots were incubated in SuperSignal West Pico Chemiluminescent substrates (Thermo Scientific, Hanover Park, IL) for 5 min and visualized with autoradiography film (Denville Scientific, Metuchen, NJ). Quantification was performed using the National Institutes of Health Image J protocol.

Statistics. Factorial analyses of variance (ANOVA) or Student *t* tests were used for between-subject comparisons involving >2 or exactly 2 levels, respectively. For analysis of *in vivo* studies on CBT one-way ANOVA with a Tukey post hoc test ($P < 0.05$) was used to determine differences in the mean among multiple groups. Area under the curve (AUC) analysis was performed using GraphPad Prism 4 Software. All results are expressed as means \pm SE.

Immunohistochemistry. Mice ($n = 4$) were deeply anesthetized with isoflurane (induction 3–5%; maintenance 1–1.5%) and placed in a Kopf stereotaxic frame (Kopf Instruments). A 33 G injector (SST-33/FT, Plastics One, Roanoke, VA) was connected to a Hamilton syringe with a polyethylene tubing and filled with Texas Red-conjugated Dextran beads (Invitrogen, Carlsbad, CA; 1 mg/ml). The injector was inserted into the dorsomedial hypothalamus (DMH) (AP = -1.58 mm, Lat = 0.25 mm; V = 4.6 mm from the surface of the brain; $n = 1$) or raphe pallidus (RPa) (AP = -6.12 mm, Lat = 0.0 mm; V = 5.8 mm from the surface of the brain; $n = 3$) according to stereotaxic coordinates (12), and 1 μ l of tracer was injected over 1 min. Animals were allowed to recover for 7 days.

Animals were perfused via the ascending aorta with 10 ml of 0.9% NaCl followed by 50 ml ice-cold 4% (wt/vol) paraformaldehyde in 0.16 mol/l PBS. Brains were removed and postfixed for 2 h in the same fixative, then transferred to PBS containing 20% (wt/vol) sucrose and stored overnight at 4°C. Sections from the POA were cut on a cryostat (Leica) at 40 μ m and transferred to individual wells containing PBS.

For indirect immunohistochemistry free-floating sections were incubated overnight with a rabbit anti-insulin receptor antibody (1:100; Pfizer PP5), rinsed in PBS, and incubated with a Donkey anti-rabbit Alexa488 (1:200; Invitrogen) for 1 h in room temperature. Sections were rinsed in PBS, followed by incubation with 0.5 μ mol/l DAPI (Invitrogen) for 5 min, then rinsed in PBS and mounted onto SuperFrost Plus slides (VWR, Ann Arbor, MI) and mounted with ProLong Gold. Confocal images were captured using a Zeiss laser confocal microscope using Zen 2009 Zeiss software suite (Carl Zeiss, Thornwood, NY). All serial optical image sections (0.3- μ m interval step slices) were imported and spatially reassembled using Imapris (Bitplane, Saint Paul, MN) to generate a three-dimensional representation of the tissue and then

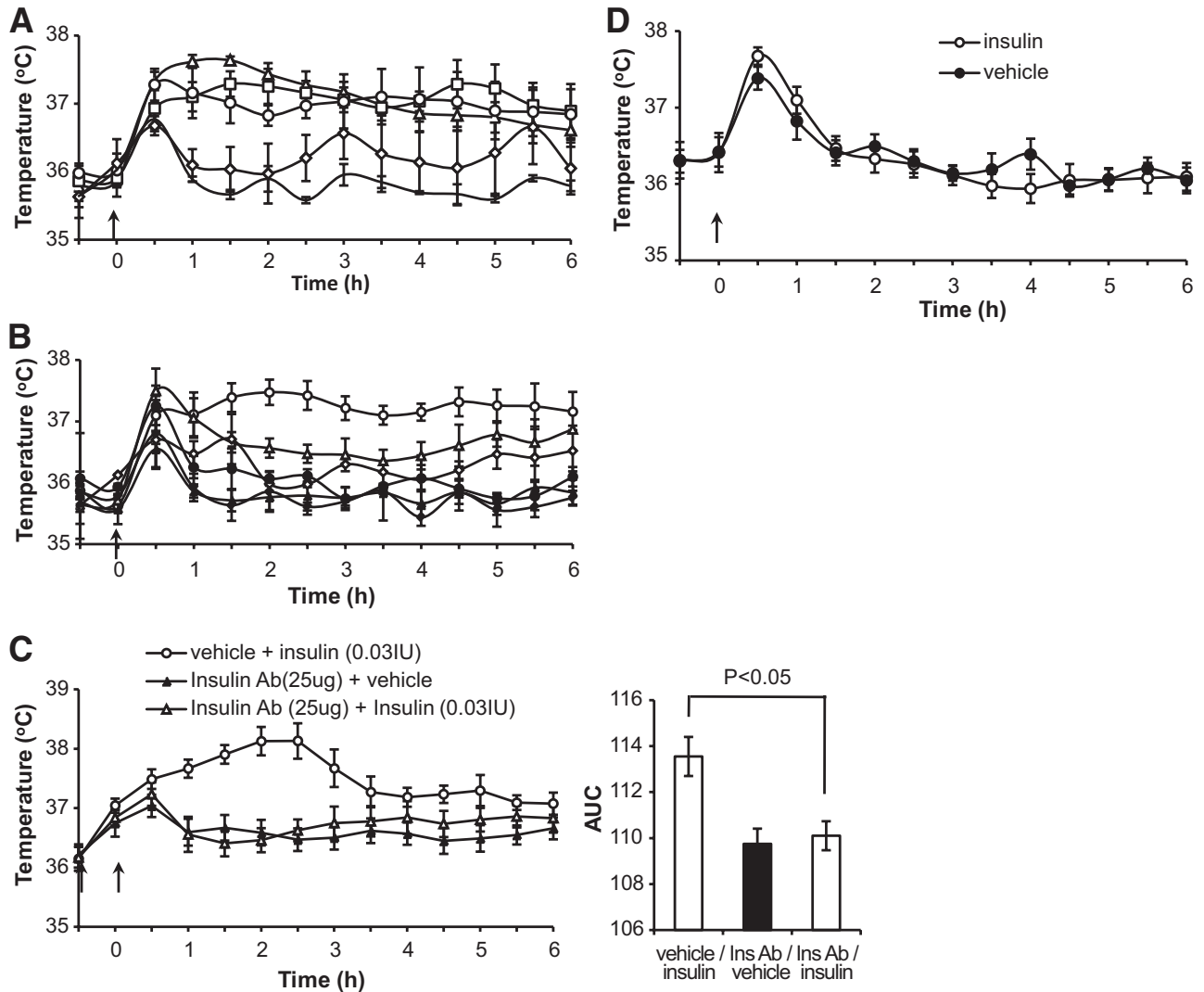


FIG. 1. Effects of central or peripheral insulin injections on CBT. **A:** Profile of the dose-dependent effects of local injection of four different doses of insulin (0.001, \diamond ; 0.015, \circ ; 0.03, \square ; and 0.06 IU, \triangle) ($n = 8$ animals per group). **B:** Graph showing the differential effects on CBT of the injection of 0.03 IU of insulin in the POA, the DMH, and the RPa (POA, \circ and \bullet ; DMH, \triangle and \blacktriangle ; RPa, \diamond and \blacklozenge ; white = insulin and black = control). **C:** Neutralizing antibody to insulin injected POA prior to insulin blocks the hyperthermic effects of insulin (insulin antibody, \triangle and \blacktriangle ; vehicle, \circ and \bullet ; white = insulin and black = vehicle). **D:** Graph showing the effects on CBT of intraperitoneal injection of 0.03 IU of insulin or vehicle. All graphs show CBT profile for the first 6 h after injection. Arrow indicates time of injection; the CBT increase observed in all conditions during the first hour is due to stress associated with injection. Data are presented as means \pm SE.

maximum projected for two-dimensional images (gray scale image panels) in Image Pro Plus (Media Cybernetics, Bethesda, MD).

RESULTS

Injection of insulin into the POA was followed by elevation of CBT lasting up to 6 h in a dose-dependent manner (Fig. 1A). Similar to mice injected with a vehicle aCSF, animals injected with insulin showed a stress-dependent elevation of CBT at time of treatment. However, CBT returned to baseline in vehicle-treated mice but not in animals that received insulin. The extent of CBT elevation was dose dependent: average CBT after injection (after stress-induced peak, from 1–6 h after injection) was $35.77 \pm 0.04^\circ\text{C}$ for vehicle and 36.21 ± 0.07 , 36.98 ± 0.03 , 37.11 ± 0.04 , and $37.08 \pm 0.11^\circ\text{C}$ (or $+0.44$, $+1.21$, $+1.34$, and $+1.31^\circ\text{C}$, respectively; $P < 0.01$) for 0.001, 0.015, 0.03, and 0.06 IU of insulin, respectively. The hyperthermic effects of insulin were significantly larger in the POA (1.34°C) than in the DMH (0.78°C) ($P < 0.01$) or the RPa (0.57°C ; $P < 0.01$), which are projection areas for the POA warm-sensitive

neurons (Fig. 1B). Pretreatment of the animals with insulin-neutralizing antibody (Fig. 1C) injected into the POA prior to injection of insulin prevented the insulin-evoked hyperthermic response. Insulin did not display hyperthermic effects when injected peripherally (intraperitoneally). The average temperature from 1–6 h after intraperitoneal injection was 36.28 ± 0.07 and $36.22 \pm 0.10^\circ\text{C}$ for vehicle and insulin (0.03 IU), respectively (Fig. 1D).

Measurement of oxygen consumption, carbon dioxide production, and the RER demonstrated that POA injection of insulin was followed by increased oxygen consumption and lower RER compared with vehicle-treated mice, indicating a switch from glucose metabolism to elevated fatty acid utilization (Fig. 2A). The lower RER upon POA insulin injection compared with that of vehicle-treated mice was prolonged and still present at 6 h postinjection. RER for vehicle and 0.03 IU insulin POA was 0.91 ± 0.02 and 0.75 ± 0.01 , respectively, ($P < 0.01$). Locomotor activity did not contribute to CBT increase because it was not affected by either vehicle or insulin injection in the POA (not shown).

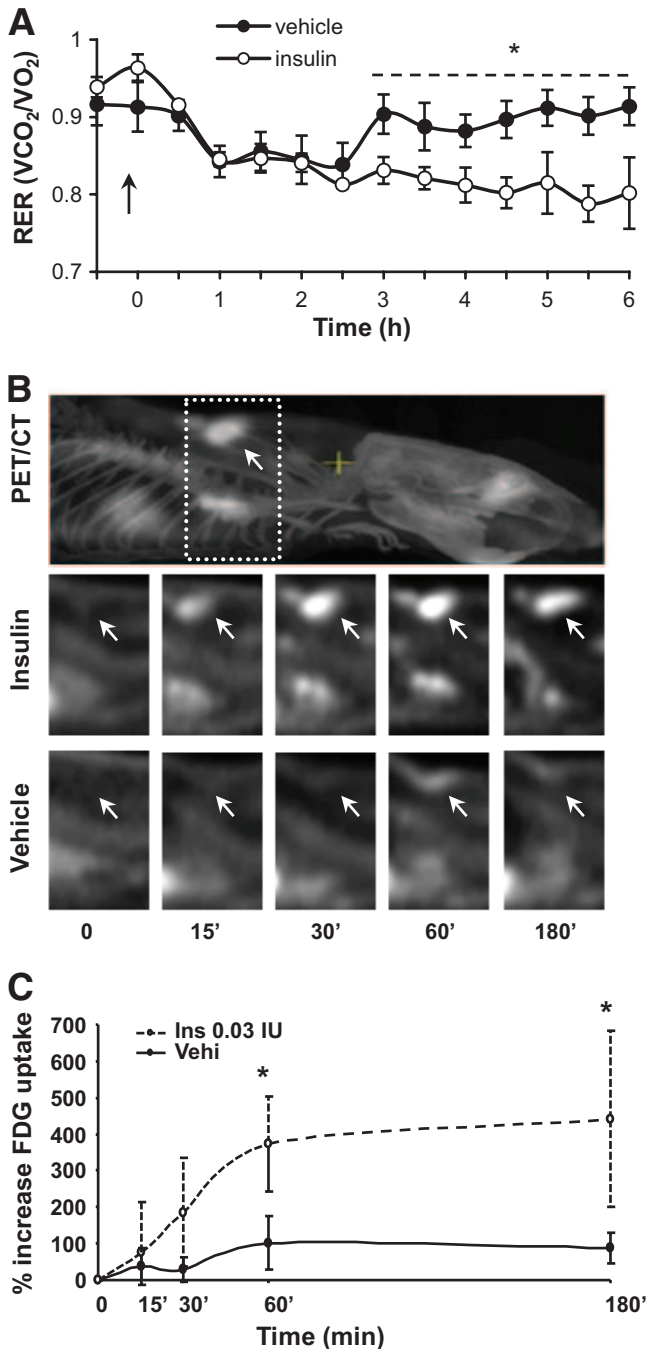


FIG. 2. POA injection of insulin increased fatty acid utilization and BAT activity **A:** The 6-h profile of RER of mice treated with vehicle or 0.03 IU insulin in the POA, demonstrating that insulin injection decreased RER, indicating an elevation of fatty acid utilization. **B:** The 3-h profile of PET/CT of ^{18}F -FDG uptake in rats injected with vehicle or 0.03 IU insulin in the POA. *Top panel* shows the representative PET/CT; squared in dotted lines is the area investigated after treatment with insulin or vehicle shown below. The anatomical position of BAT is indicated with an arrow. **C:** The 3-h profile quantification of ^{18}F -FDG uptake into BAT after insulin treatment as indicated. Data are presented as means \pm SE. * $P < 0.05$.

PET and CT imaging carried out on rats demonstrated that insulin injected into the POA activated BAT thermogenesis because the insulin treatment induced up to fivefold ($P < 0.05$) elevation in BAT glucose ^{18}F -FDG uptake (Fig. 2B and C). Because in the arcuate nucleus, insulin was shown to activate the PI3K pathway (13), the hyperthermic effects of insulin into the POA were also assessed in the presence

of a PI3K-I. Pretreatment with PI3K-I LY294002 (10 nmol in 0.5 μl) before insulin (0.03 IU), both administered to the POA 20 min apart, showed significant attenuation of insulin-induced hyperthermia ($P < 0.01$) (Fig. 3A). Comparison of the area under the curve (AUC) for pretreatment with PI3K-I followed by either insulin or vehicle did not elicit statistically significant results. The peak hyperthermic response to insulin administered to the POA was observed 2 h after the pretreatment injection of vehicle. At this time point pretreatment with PI3K-I reduced the insulin-induced temperature elevation by 1.4°C (from 2.03 to 0.63°C) (Fig. 3A).

Biochemical analysis of POA tissues confirmed the presence of the insulin receptor in the POA. Comparative analysis demonstrated that insulin (0.03 IU) treatment induced an elevation of the activated phosphorylated form of AKT(Ser 437): the level of pAKT increased $317 \pm 82.7\%$ compared with vehicle 90 min after the injection (Fig. 3B), which is in line with the involvement of PI3K in the insulin signaling in this hypothalamic area.

The hypothesis, suggested by the presence of the insulin receptor transcript found by single-neuron chipping of individual warm-sensitive neurons in the POA (in preparation), that insulin might act directly on warm-sensitive neurons was also tested by electrophysiological recording of the effects of insulin on primary warm-sensitive PO/AH anterior hypothalamus (AH) neurons (WSN) in hypothalamic slices. Insulin was locally applied to warm-sensitive PO/AH neurons using a microperfusion tip. WSNs were identified by measuring the change in the firing rate during a temperature ramp; the thermal coefficient of the WSNs was $0.93 \text{ impulses s}^{-1} \text{ C}^{-1}$ (Fig. 4A and B) as previously described (14). Insulin (0.3 IU/ml) decreased the firing rate of the WSN from 1.1 to 0.3 Hz (i.e., by 73%) (Fig. 4C). Similar experiments revealed that the firing rates for 9 of 19 (43%) warm-sensitive PO/AH neurons tested were reversibly inhibited by insulin (0.3 IU/ml). The decrease in firing rate averaged $54 \pm 19\%$ ($n = 9$). The firing rate averaged $4.9 \pm 2.6 \text{ Hz}$ ($n = 9$) in control and $2.6 \pm 2.4 \text{ Hz}$ ($n = 9$) in the presence of insulin. This effect was accompanied by a hyperpolarization of $3.2 \pm 2.7 \text{ mV}$ ($n = 9$). At 0.15 IU/ml insulin reduced the firing rate of warm-sensitive PO/AH neurons by $10 \pm 7\%$ ($n = 3$). These effects are consistent with the current models of central thermal regulation that state that the PO/AH sends an inhibitory γ -aminobutyric acid (GABA)ergic signal to the thermoregulatory centers DMH and/or RPa and controls thermogenesis induced by local or skin cooling or by binding of pyrogens to their receptors on warm-sensitive neurons (10). Thus, inhibition of neuronal activity in the PO/AH results in hyperthermia, whereas a decrease in activity results in hypothermia (reviewed in [15]). As predicted by this model, insulin-induced inhibition of the activity of PO/AH warm-sensitive neurons resulted in hyperthermia.

We then tested whether insulin caused hyperpolarization and whether reduction in firing rate involved the activation of ATP-sensitive K^+ channels (K_{ATP} channels) as previously described on insulin effects in the arcuate neurons (5). The K_{ATP} channel blocker glibenclamide (20 $\mu\text{mol/l}$) was applied to the bath for 5 min prior to local insulin application. The channel blocker increased the firing rate of all neurons tested by $21 \pm 15\%$ ($n = 6$) (Fig. 4D and E). The presence of glibenclamide blocked the previously observed inhibitory effect of insulin (0.3 IU/ml) on the firing rate in warm-sensitive POA/AH neurons (Fig. 4D and E). The PI3K-I LY249002 (5 $\mu\text{g/min}$ bath) inhibits the

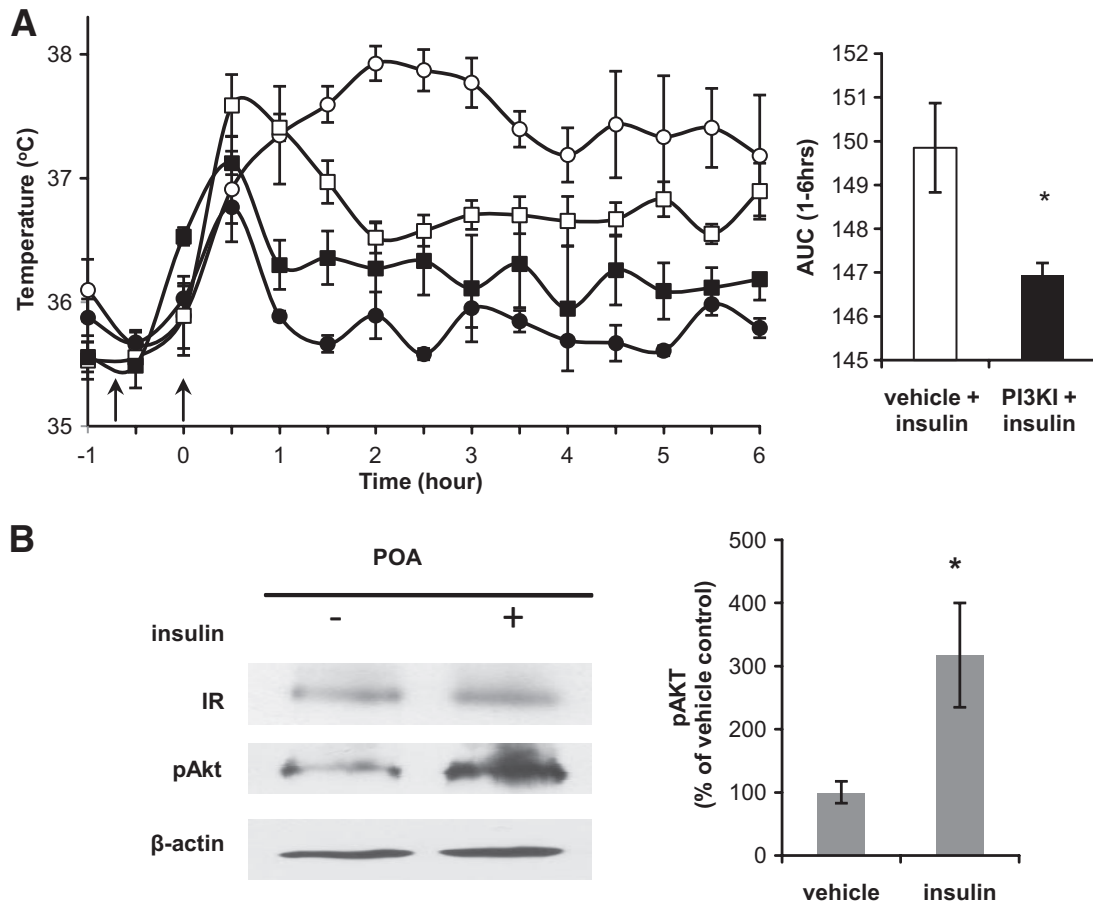


FIG. 3. The hyperthermic effects of POA injection of insulin are inhibited by the PI3K-I and induce an elevation of the activated phosphorylated form of AKT. **A:** The 6-h profile of the effects of PI3K-I treatment on insulin-induced elevation of CBT. Animals were pretreated with 10 nmoles of PI3K-I in 0.5 μ l 20 min before injection of 0.03 IU of insulin; arrows indicate time of injections (PI3K-I, \square and \blacksquare ; vehicle, \circ and \bullet ; white = insulin and black = vehicle). **B:** Western blot analysis of POA tissues confirmed the presence of the insulin receptor in the POA; the level of pAKT increased 317 + 82.7% compared with vehicle 90 min after the injection of insulin to the POA. Data are presented as means \pm SE. * $P < 0.05$.

in vivo hyperthermic effects of insulin (Fig. 1C) and also prevents the insulin-induced inhibition of the firing rate of the WSNs in the POA. The inhibitory effect of LY249002 on insulin's action (Fig. 4F and G) suggests that at least some of the effects of insulin in the POA are exerted at the level of regulating the firing rate of WSNs and, through this mechanism, the level of BAT activation and thermogenesis. No effects of leptin (0.1 μ mol/l) and hypoglycemia (glucose 10–1 mmol/l) on the activity of WSN were observed (data not shown), although in other hypothalamic nuclei there are interactions among glucose, leptin, and insulin signaling.

Retrograde tracing from the RPa (Fig. 5A) or DMH (not shown) show labeled neurons in the POA. Immunohistochemical detection of the insulin receptor shows colocalization with retrogradely traced neurons projecting to the RPa (Fig. 5A–E) as well as adjacent insulin receptor-positive only neurons (Fig. 5E).

DISCUSSION

Injection of insulin into the preoptic area of the hypothalamus induced a specific and dose-dependent elevation of CBT mediated by stimulation of BAT thermogenesis as shown by imaging and RER measurement. These data show how insulin, primarily known for its peripheral action as a regulator of glucose uptake, may act as a central stimulator of fatty acid oxidation in BAT. Retro-

grade tracing indicates that insulin receptor-expressing warm-sensitive neurons activate BAT through projection via the RPa. WSNs are functional components of the neuronal circuitry that regulate temperature homeostasis. These neurons are known to respond to local changes in temperature and to pyrogens during infection or diseases. Insulin applied on hypothalamic slices acted directly on intrinsically warm-sensitive neurons by inducing hyperpolarization and reducing firing rates. It should be noted that the POA insulin doses used give rise to POA insulin concentrations that are in the range of circulating plasma concentrations of insulin and are unlikely to exert the BAT effects via leakage to other brain areas or to the periphery. However, not all WSN tested responded to insulin, and none responded to leptin or changes in glucose concentrations (not shown), indicating that WSNs constitute a heterogeneous population of neurons and that insulin inhibits only a subset of these POA neurons; however, this subset represents an input potent enough to the BAT regulation to cause a hyperthermic response. The insulin-sensitive WSNs may mediate actions important for the energy balance and may participate in the thermic effects of food, a phenomenon inversely correlated to the degree of insulin resistance and of body fat and proposed to be important in the development of obesity (16). Our data show how insulin can affect BAT activity via central action on warm-sensitive neurons. This is important in light of

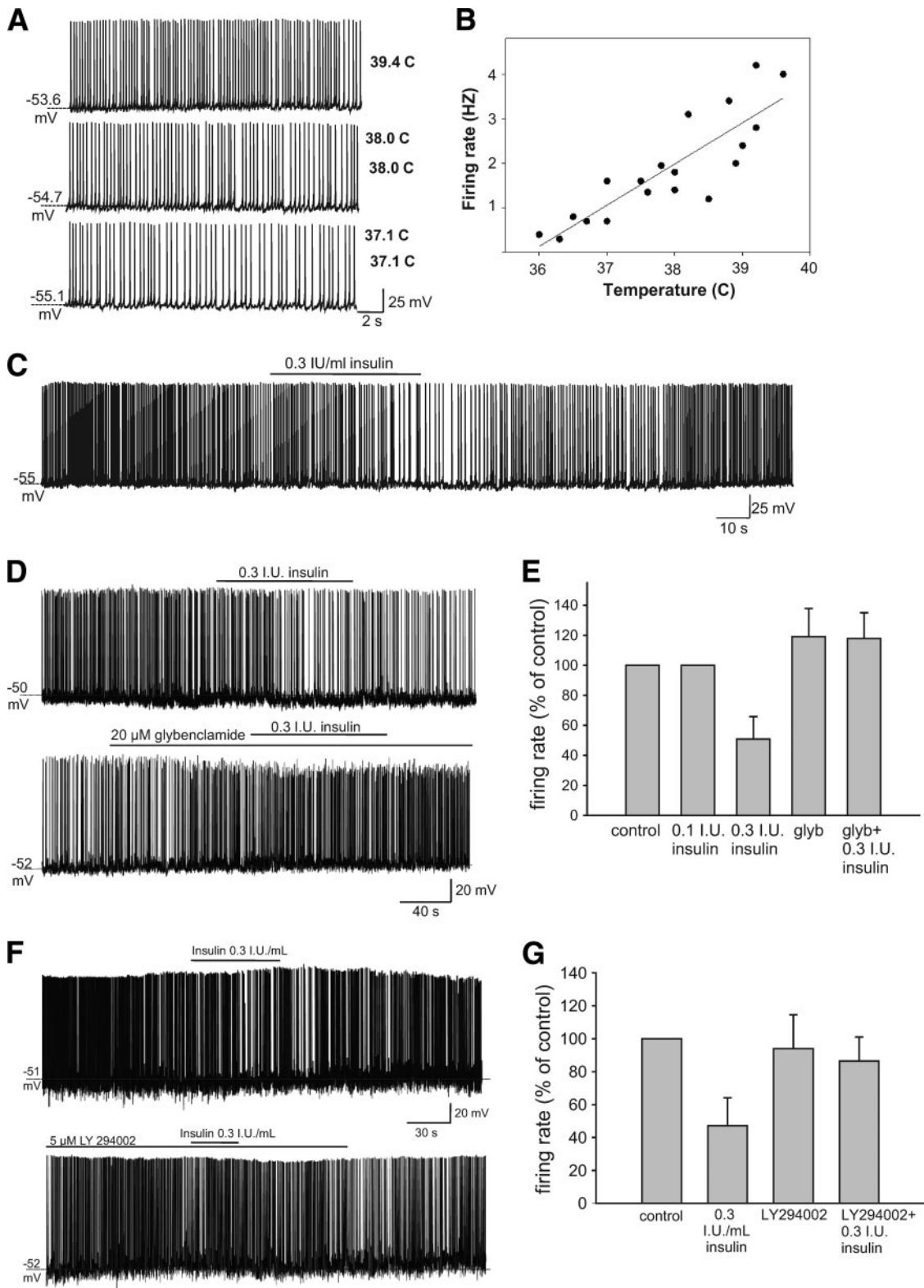


FIG. 4. Effects of temperature and insulin on the firing-rate activity of a PO/AH warm-sensitive neuron and the role of K_{ATP} channels and PI3K in the inhibitory effects of insulin on warm-sensitive PO/AH neurons. **A:** Spontaneous firing activity of a PO/AH neuron at three different temperatures. **B:** Firing rate versus temperature plot. The slope of the linear regression, indicated by the solid line, is $0.93 \text{ impulses s}^{-1} \text{ } ^\circ\text{C}^{-1}$. **C:** Application of insulin (0.3 IU/ml) induced a small hyperpolarization (2mV) and decreased the firing rate of the neuron from 1.1 to 0.3 Hz. **D:** Bath application of the K_{ATP} channel blocker glybenclamide (20 $\mu\text{mol/l}$) reduced the firing rate of WSNs by 43%. In the presence of the K_{ATP} blocker, insulin (0.3 IU/ml) did not affect the firing rate of WSNs. **E:** Bar chart summarizing the effect of insulin (0.3 IU/ml, $n = 9$; 0.1 IU/ml; $n = 5$), glybenclamide (20 $\mu\text{mol/l}$; $n = 6$), and insulin (0.3 IU/ml, $n = 6$) in the presence of the blocker. **F** and **G:** Bath application of the PI3K-I LY294002 (5 $\mu\text{mol/l}$) prevents the insulin- (0.3 IU/ml; $n = 6$) caused inhibition of firing rate (**F**). Data are presented as means \pm SE.

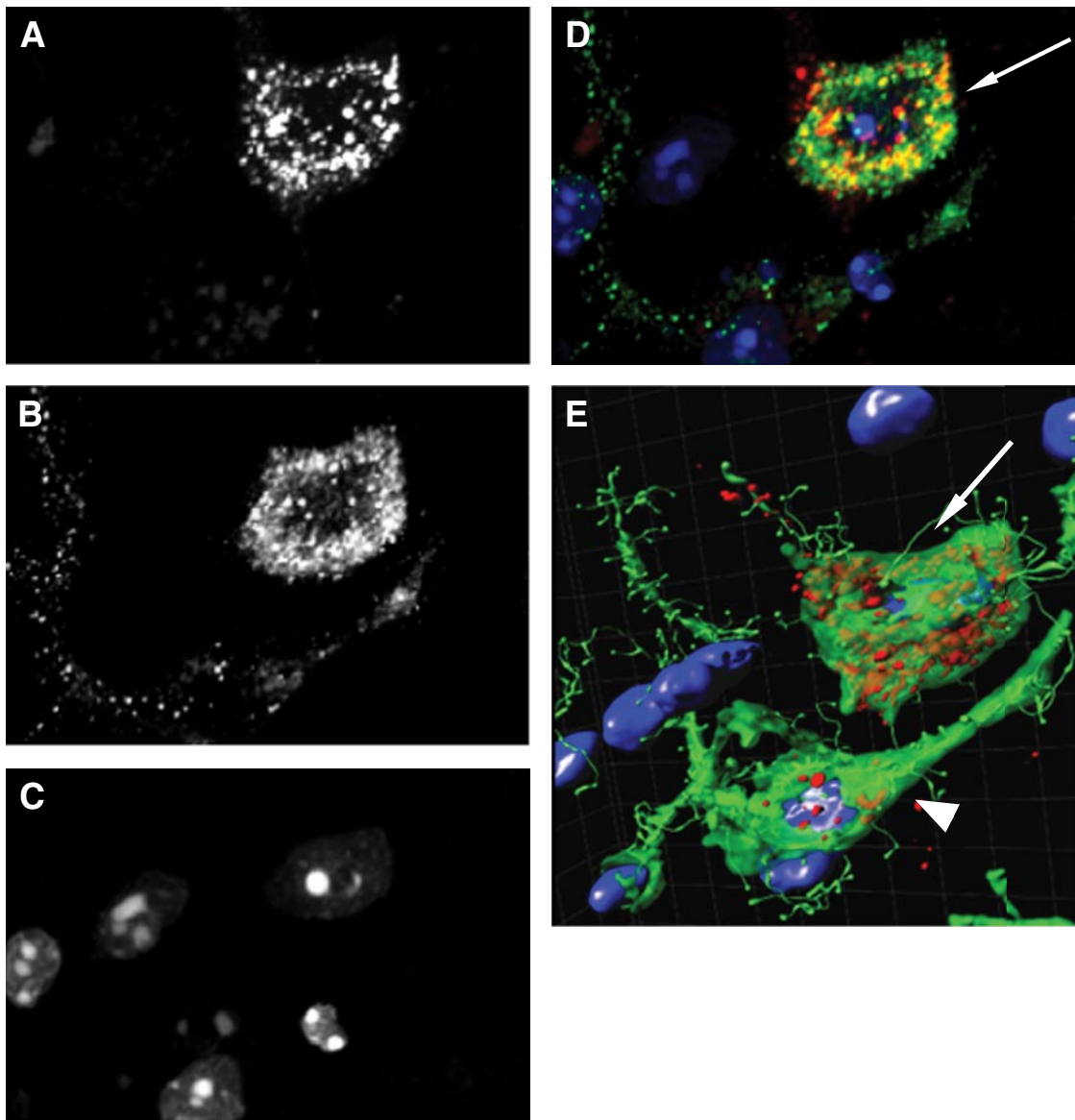


FIG. 5. Insulin receptor–positive neurons identified by retrograde tracing from the RPa. *A–D*. Texas Red tracer (*A*, red in *D* and *E*) is colocalized with the insulin receptor (*B*, green in *D* and *E*) and the nucleus stained with DAPI (*C*, blue in *D* and *E*). *E*: A three-dimensional reconstruction of the same neuron as seen in *A–D* showing an insulin receptor–positive traced neuron (arrow in *D* and *E*) and an insulin receptor only positive neuron (arrowhead). All images were captured with a 63 \times magnification. (A high-quality color digital representation of this figure is available in the online issue.)

recent findings on the role of BAT activity in diabetes and in obesity (17,18). The demonstration that WSNs in the POA respond directly to insulin with increased thermogenesis provides an important link between thermoregulation and energy homeostasis.

ACKNOWLEDGMENTS

This study was supported by The Harold L. Dorris Neurological Research Institute, The Skaggs Institute for Chemical Biology, The Ellison Medical Foundation, Pfizer (SFP1729), the National Institutes of Health (Grants R01NS043501, R01NS060799, DP1-OD-04117, AG 9900, and AG028040), and by Health Research Formula Funds from the Commonwealth of Pennsylvania.

J.E. is an inventor on the aRNA Amplification Technology patent, which is licensed to LBS Technologies, a company on which J.E. serves on the scientific advisory board. The company has commercialized the aRNA ampli-

fication procedure used to generate microarray probes and sequencing templates in this article. No other potential conflicts of interest relevant to this article were reported.

Parts of this study were presented in abstract form at the 2nd International Meeting on Physiology and Pharmacology of Temperature Regulation, Matsue, Japan, 23–26 July 2009.

REFERENCES

1. Boulant JA. Role of the preoptic-anterior hypothalamus in thermoregulation and fever. *Clin Infect Dis* 2000;31(Suppl. 5):S157–S161
2. Hammel HT, Hardy JD, Fusco MM. Thermoregulatory responses to hypothalamic cooling in unanesthetized dogs. *Am J Physiol* 1960;198:481–486
3. Nakayama T, Hammel HT, Hardy JD, Eisenman JS. Thermal stimulation of electrical activity of single units of the preoptic region. *Am J Physiol* 1963;204:1122–1126
4. Leibowitz SF, Wortley KE. Hypothalamic control of energy balance: different peptides, different functions. *Peptides* 2004;25:473–504

5. Plum L, Schubert M, Brüning JC. The role of insulin receptor signaling in the brain. *Trends Endocrinol Metab* 2005;16:59–65
6. Wang HS, Lin MT. Effects of insulin on thermoregulatory responses and hypothalamic neuronal activity. *Pharmacology* 1985;30:86–94
7. Cardona-Gómez GP, DonCarlos L, Garcia-Segura LM. Insulin-like growth factor I receptors and estrogen receptors colocalize in female rat brain. *Neuroscience* 2000;99:751–760
8. Unger J, McNeill TH, Moxley RT, 3rd, White M, Moss A, Livingston JN. Distribution of insulin receptor-like immunoreactivity in the rat forebrain. *Neuroscience* 1989;31:143–157
9. van Baak MA. Meal-induced activation of the sympathetic nervous system and its cardiovascular and thermogenic effects in man. *Physiol Behav* 2008;94:178–186
10. Nakamura K, Morrison SF. A thermosensory pathway that controls body temperature. *Nat Neurosci* 2008;11:62–71
11. Tatsumi M, Engles JM, Ishimori T, Nicely O, Cohade C, Wahl RL. Intense (18)F-FDG uptake in brown fat can be reduced pharmacologically. *J Nucl Med* 2004;45:1189–1193
12. Paxinos G, Franklin KBJ. *The Mouse Brain in Stereotaxic Coordinates*. 2nd ed. San Diego, CA, Academic Press, 2008
13. Niswender KD, Morrison CD, Clegg DJ, Olson R, Baskin DG, Myers MG Jr, Seeley RJ, Schwartz MW. Insulin activation of phosphatidylinositol 3-kinase in the hypothalamic arcuate nucleus: a key mediator of insulin-induced anorexia. *Diabetes* 2003;52:227–231
14. Tabarean IV, Conti B, Behrens M, Korn H, Bartfai T. Electrophysiological properties and thermosensitivity of mouse preoptic and anterior hypothalamic neurons in culture. *Neuroscience* 2005;135:433–449
15. Morrison SF, Nakamura K, Madden CJ. Central control of thermogenesis in mammals. *Exp Physiol* 2008;93:773–797
16. de Jonge L, Bray GA. The thermic effect of food and obesity: a critical review. *Obes Res* 1997;5:622–631
17. Cypess AM, Lehman S, Williams G, Tal I, Rodman D, Goldfine AB, Kuo FC, Palmer EL, Tseng YH, Doria A, Kolodny GM, Kahn CR. Identification and importance of brown adipose tissue in adult humans. *N Engl J Med* 2009;360:1509–1517
18. Virtanen KA, Lidell ME, Orava J, Heglund M, Westergren R, Niemi T, Taittonen M, Laine J, Savisto NJ, Enerbäck S, Nuutila P. Functional brown adipose tissue in healthy adults. *N Engl J Med* 2009;360:1518–1525